A Low Cost Solution for NOAA Remote Sensing

Conference Paper · January 2018

DOI: 10.5220/0006639101280134

CITATIONS
2

READS
621

4 authors:

Edoardo Ardizzone
Università degli Studi di Palermo
185 PUBLICATIONS **1,721** CITATIONS
SEE PROFILE

Alessandro Bruno
IULM Libera Università di Lingue e Comunicazione di Milano
95 PUBLICATIONS **682** CITATIONS
SEE PROFILE

Francesco Gugliuzza
Expleo Italia S.p.A.
8 PUBLICATIONS **32** CITATIONS
SEE PROFILE

Roberto Pirrone
Università degli Studi di Palermo
173 PUBLICATIONS **1,066** CITATIONS
SEE PROFILE

A Low Cost Solution for NOAA Remote Sensing

Edoardo Ardizzone, Alessandro Bruno, Francesco Gugliuzza and Roberto Pirrone
Dipartimento dell'Innovazione Industriale e Digitale (DIID), Università degli Studi di Palermo,
Viale delle Scienze Ed. 6 - 90128 Palermo (PA), Italy
{*edoardo.ardizzone, alessandro.bruno15, francesco.gugliuzza, roberto.pirrone*}*@unipa.it*

Keywords: Remote Sensing, Satellite Communication, Signal Processing.

Abstract: United States National Oceanic and Atmospheric Administration (NOAA) weather satellites adopt Advanced Very High Resolution Radiometer (AVHRR) sensors to acquire remote sensing data and broadcast Automatic Picture Transmission (APT) images. The orientation of the scan lines is perpendicular to the orbit of the satellite. In this paper we propose a new low cost solution for NOAA remote sensing. More in detail, our method focuses on the possibility of directly sampling the modulated signal and processing it entirely in software enabled by recent breakthroughs on Software Defined Radios (SDR) and CPU computational speed, while keeping the costs extremely low. We aim to achieve good results with inexpensive SDR hardware, like the RTL-SDR (a repurposed DVB-T USB dongle). Nevertheless, we faced some problems caused by hardware limits such as high receiver noise figure and low ADC resolution. Furthermore, we detected several inherent drawbacks of frequent tuner saturations. For this purpose we developed a software-hardware integrated system able to perform the following steps: satellite pass prediction, time scheduling, signal demodulation, image cropping and filtering. Although we employed low cost components, we obtained good results in terms of signal demodulation, synchronization and image reconstruction.

1 INTRODUCTION

Airborne and satellite sensors allow us to analyze a huge amount of data used for many tasks such as signal and image processing for GIS applications, weather and storm predictive analysis, earth observation and more generally, remote sensing. Everyday several United States National Oceanic and Atmospheric Administration (NOAA) weather satellites pass over us: each NOAA weather satellite broadcasts an Automatic Picture Transmission signal, which contains a live weather image of the area overflown by the satellite. The satellite scanner systems include line scanning devices observing the earth perpendicular to the orbital plane. The signal measurements are performed in different spectral bands thanks to the Advanced Very High Resolution Radiometer (AVHRR) instrument. The visible light and the infrared images are combined in a row vector; the combination is done using the Automatic Picture Transmission (APT) system.

Although many scientific progresses have been made, there are still many open scientific challenges for NOAA satellites, such as information calibration or the physical layer (synchronization, data detection, channel codec). Many satellite-based platforms are dedicated to remote sensing data analysis for weather prediction as well as for climatological studies. In this paper we present a new easily accessible satellite based platform for signal processing, installed in our lab: the platform consists of a low cost receiver subsystem for public weather satellites and a signal processing subsystem for different applications (image reconstruction, image enhancement and clouds segmentation). The rest of the paper is organized as it follows: in section 2 we describe the state of the art methods for satellite signals modulation and imagery, in section 3 we show in greater detail our proposed platform for the reception of NOAA signals, in section 4 we show the experimental results for the reconstructed images and the section 5 ends the paper with conclusions and future works.

2 STATE OF THE ART

In this section we give a description of the state of the art of the techniques for the demodulation of signals coming from NOAA satellites. Furthermore, a brief overview of the image processing techniques for clouds detection is given.

Ardizzone, E., Bruno, A., Gugliuzza, F. and Pirrone, R.
A Low Cost Solution for NOAA Remote Sensing.
In *Proceedings of the 7th International Conference on Sensor Networks (SENSORNETS 2018)*, pages 128-134
ISBN: 978-989-758-284-4

2.1 Satellite Communications and Signals Reception

Artificial satellite development was originally fuelled by the need for superpowers to show their ”status” to their opponents, during the Space Race. After a few years, however, it became clear that satellites could be used to establish a reliable communication infrastructure or for remote sensing. In the last decades many communications satellites were launched into space: some of them are equipped with low bandwidth communication systems (VHF/UHF), while some others are equipped with high bandwidth communication systems (even more recently, communications are carried out by arrays of high bandwidth microwave transponders, designed to offer multimedia services (Farserotu and Prasad, 2000)). Modern satellites receive and transmit simultaneously thousands of signals: hyperspectral cameras and radiometers have been widely used to analyze Earth's visible and infrared radiation directly from the spacecraft; Synthetic Aperture Radars (SAR) have been used to map surface features and texture, even through cloud cover. The result is the possibility to analyze data like vegetation moisture (to estimate wildfire risk) (Al-Moustafa et al., 2012) or reconstruct 3D models of confined zones of the Earth (recently even at 1-meter resolution). Due to sensor nonlinearities, raw sensor data can be affected by noise and distortions, and needs to be corrected with classification or regression methods (Camps-Valls et al., 2011).

The APT format used by NOAA satellites was first introduced in the 1960s (Barnes and Smallwood, 1982) (Winston, 1997) and has been only slightly modified since, so it's no surprise that many stations still use analog-radio equipment designed in the 1980s or the 1990s. The APT signal is formed by amplitude modulating a 2400 Hz carrier with each line of pixel data obtained by merging two images and calibration data (see subsection 3.1), and then frequency modulating the result; it is obvious that the ease of building a basic receiver composed of a FM demodulator followed by an AM demodulator and an analog-digital converter has sparked the interest of many scientists and amateur radio operators. However, receiving and demodulating signals coming from satellites not placed in geostationary orbits presents many challenges because the radio wave itself changes frequency due to Doppler effects and free space attenuation is not constant but, instead, varies with distance from the satellite. Another problem is that due to satellites' variable rotation relative to Earth's axis, linearly polarized antennas become unsuitable and circularly polarized antenna are required to ensure reliable and effective demodulation and synchronization, as well as a good quality output image.

Image synchronization and calibration, unlike demodulation and frequency tracking, are usually performed in software instead of hardware (Benabadji et al., 2004) because they are non-real time tasks that require some CPU power (mainly signal down sampling, synchronization pulse convolution and line-by-line pixel value processing); it is also important to say that it would be somewhat challenging to implement those tasks in hardware (at least for non-experts). Sensor data can then be further corrected to compensate small sensor alignment errors, orbit uncertainty and on-board clock offset, by comparing expected and measured emissivity over land and sea and binning results into a high-resolution grid (Moradi et al., 2013).

2.2 Clouds Segmentation

The accurate separation of clouds from lands in satellite imagery is a critical step, due to the varying conditions of surface properties, such as reflectance and emissivity. Furthermore, the classification of the cloud types from satellite imagery is useful for weather research and forecast applications (forecasting of meteorological phenomena) (Feidas et al., 2000). Heidinger et al. in (Heidinger et al., 2012) performed a naive Bayesian approach for cloud detection. This kind of methodology has been used for cloud detection on NOAA AVHRR data. Generally, NOAA AVHRR sensors have coarser spatial resolution than most modern satellites. Some methods face the problem of the enhancement of NOAA AVHRR data (such as remote sensing images). In (Alkhatib et al., 2012) the authors used region growing method for dust clouds segmentation. In (Karlsson et al., 2015) the authors examined two probabilistic methods for cloud masking of images from NOAA satellites, obtained with Advanced Very High Resolution Radiometer.

Simpson and Gobat in (Simpson and Gobat, 1996) used AVHRR Split-and-Merge Clustering (ASMC) for cloud detection to overcome the problem of varying land surface reflectance and emissivity. Split-and-merge clustering allows to segment the scene in its natural groupings and label them as cloud, cloud-free land, uncertain. In (Yhann and Simpson, 1995) the authors performed a supervised approach based on neural networks for cloud screening of AVHRR data over the ocean. In our work the signals coming from NOAA satellites are demodulated, synchronized and enhanced by using image processing techniques (see section 4), then clouds detection is performed by using the Otsu's method (Zhang and Hu, 2008).

3 PROPOSED METHOD

Our method focuses on the possibility of directly sampling and processing of the modulated signal entirely in software enabled by recent breakthroughs on Software Defined Radios (SDR) and CPU computational speed. Our objective was achieving good results with inexpensive SDR hardware like RTL-SDR (Sruthi et al., 2013) (a repurposed DVB-T USB dongle), high receiver noise figure and low ADC resolution. We also dealt with the inherent drawbacks caused by frequent tuner saturations. An integrated hardware and software system is proposed to perform satellite pass prediction, time scheduling, signal demodulation, image filtering.

3.1 APT Signal

The APT was introduced in 1960s and it shows its age in some respects: it is a mixed modulation signal (AM+FM) carrying a completely analog payload. The standard APT format consists of around 2080 pixels row, which is divided in two sub-rows of 909 pixels each belonging to two different sub-images (A and B) and then padded with synchronization and diagnostic information words. Images A and B during daytime are acquired in the visible range and in the infrared range of the electromagnetic spectrum respectively. At night-time, image A is replaced with one acquired at an infrared wavelength different from that of B. Rows can be grouped logically in frames of 128 lines each: a complete frame contains image calibration data and dynamic range references (wedges) (Winston, 1997). The payload is used to amplitude modulate a 2400 Hz carrier according to (1)

$$s(t) = [1 + m(t)]\, A\, \cos(2\pi f_c t) \tag{1}$$

Where m(t) is the modulating signal, A the carrier's amplitude and f_c the carrier's frequency. The amplitude modulated signal is then frequency modulated with a frequency deviation of about 18-20 kHz and transmitted in the 137 MHz band at about 5 W EIRP (36.99 dBm) and 4160 sym/s symbol rate. Right hand circularly polarized (RHCP) antennas transmit the signal, so particular care had to be taken when choosing which antenna type to use in the receiving station.

3.2 Hardware

First of all we build a circularly polarized antenna: the "turnstile" crossed-dipoles design was chosen because of its simplicity and the good performance provided when placed over a ground plane. Ease of construction, durability and suitability of common materials compensate the drawbacks of the system: the medium gain offered (6 dBi) and many nulls present in such a design (Griffiths, 2014). The antenna has been built exclusively off PVC pipes, threaded bars as dipole elements, nuts and bolts and 75 Ω generic coaxial cable. The antenna is directly connected to a repurposed old TV amplifier (SIEL .269 01), modified to behave like a wide-bandwidth amplifier. The input variable attenuator and high-pass filter have been removed, and the RF output has been separated from DC power path, allowing power without a bias tee. The amplifier uses two active components:

- BFR90A - 16 dB gain, 1.8 dB NF
- BFR91A - 14 dB gain, 1.6 dB NF

The results are 30 dB gain and ~1.52 dB NF (calculated using Friis' formula (Promwong and Takada, 2004)). Ignoring noise introduced by amplifier's passive components, and considering room temperature of 290 K and 40 kHz bandwidth, the noise output of the amplifier can be calculated with formula (2).

$$N_{in} + g + NF \tag{2}$$

N_{in} is the input noise (-127.95 dBm) calculated using formula (3), g the gain (30 dB) and NF the total noise figure (1.52 dB). The result is a noise output of -96.43 dBm.

$$10\log_{10}(kTB) + 30 \tag{3}$$

k is Boltzmann constant, T is absolute temperature and B is signal bandwidth, while +30 has been added to convert results from dBW to dBm. Considering NOAA satellites transmit at 5 W EIRP, when they are at receiving station's zenith the signal power at the receiver's input can be calculated as follows

$$\begin{aligned} &\text{36.99 dBm - 133.34 dB + 6 dBi - 3 dB + 30 dB =} \\ &\qquad = \text{-63.35 dBm} \end{aligned} \tag{4}$$

133.34 dB is free space loss and 3 dB is the estimated loss due to cable and connectors. Output SNR in best-case conditions is then 33.08 dB, more than enough to ensure good image quality. The amplifier's output is connected to a SAW filter (Tai-Saw TA1581A) centered on 137.5 MHz to attenuate out-of-band signals and reduce the severe distortion caused by high-power FM broadcast stations and GSM signals. The TA1581 is a 50 Ω device, but an impedance matching circuit has not been installed because of the low mismatch loss (0.177 dB from antenna to filter and another 0.177 dB from filter to next RF device, which has 75 Ω impedance) compared to filter's 3.5 dB insertion loss. We added a standard ferrite bead near the receiver to shield common-mode interference caused by

high-frequency equipment (PC, lab instruments, electronic ballasted lamps, etc.). The SDR hardware is widely available at a very low cost and is built around two chips: a RF tuner and an ADC/COFDM demodulator combo chip. The first used to be an Elonics E4000 (zero-IF), but has been replaced on new models with two superheterodyne alternatives, the Rafael Micro R820T and R820T2. The demodulator chip, a Realtek RTL2832U, is commonly used to demodulate the QPSK or QAM DVB-T signal into a MPEG stream and send it to a PC via an USB interface, but has a hidden passthrough mode which allows passing the ADC sample stream instead. The samples are internally filtered by a 32 coefficients FIR filter. For this study a dongle containing an E4000 tuner has been used.

3.3 Software

Managing tuner's and RTL2832U's hardware registers is not an easy task, and it has been hindered by the lack of a public datasheet for the Realtek chip, but the RTL-SDR team has coded a very efficient open source C library which abstracts from hardware difficulties (Osmocom, 2012), allowing developers to tune the receiver and get ADC samples with few function calls. Thanks to the Mathworks RTL-SDR library we focused on the development of DSP algorithms on Simulink (Sergienko, 2014), taking advantage of its model-to-code conversion functionality. The FM demodulation was initially delegated to Kyle Keen's rtl_fm (Keen, 2013) software, but it was plagued by frequent saturation problems. It was then decided to implement a simple FM demodulation algorithm directly in the Simulink model. The software developed consists of the following parts: satellite pass predictor, digital down-converter, FM demodulator, FIR low-pass filter, AM demodulators, synchronization block, pixel dynamic range calibration block, model's parameters generator.

3.3.1 Satellite Pass Predictor

The first step in obtaining a completely automatic system was to develop a method to automatically schedule the appropriate start time for the receiving/demodulating software. John Magliacane's PREDICT (Magliacane, 2001) software has been used to predict start/end times and maximum elevations of the next satellite passes. This software supports command line parameters and text output, enabling the execution of a script for multiple pass predictions. PREDICT's output is processed in order to make it compatible with Microsoft Windows schtasks.exe syntax, but it can be easily modified to use Linux/UNIX cron instead.

3.3.2 RTL-SDR Library for Simulink

The library used in this work includes the DLL files for hardware-software communication, the required precompiled code to interface them with MATLAB and a source block that has to be added to Simulink models.

3.3.3 Digital Down-converter

It was necessary to overcome the DC offset issue caused by the Zero-IF tuner architecture, so we designed and implemented an offset tuning mechanism. The RTL-SDR is tuned 500 kHz lower than the target frequency, and a Simulink block performs a circular frequency shift to shift the desired signal back to baseband using (5).

$$e^{-j\Omega_0 n} = e^{\frac{-j2\pi f_0 n}{fs}} \tag{5}$$

3.3.4 FM Demodulator

There are many examples of DSP FM demodulators in literature, some of which use the computationally expensive arctangent function. Experimental test showed that the non-CPU intensive demodulator presented in (Lyons, 2004) (capable of scaling the output signal according to input modulus amplitude) was inappropriate as it caused uncontrolled phase shift in the demodulated output, preventing correct APT format decoding. Therefore an arctangent-based demodulator (Shima, 1995) was chosen (equipped with a signal scaler), as shown in Fig. 1.

3.3.5 Low-Pass FIR Filter

A linear phase FIR filter designed using a Kaiser window has been added to the Simulink model in order to attenuate noise present in the FM demodulator output. Its optimal cutoff frequency (5000 Hz) has been found experimentally and varies with hardware receiver and FM demodulation algorithm characteristics.

3.3.6 AM Demodulators

We developed two DSP AM demodulators (Fig. 1): the first is based on a discrete-time PLL followed by a low-pass filter with a cutoff of 1500 Hz to attenuate $2\pi f_c$ frequency components. As with any PLL, its performance is determined to a large extent by Ki and Kp coefficients (a wrong choice leads to instability, especially with low SNR signals). Initially, FIR filter delay in the feedback path was considered when

choosing coefficients' values, as in (Wilson et al., 2009), but unsatisfactory experimental results suggested a different approach was necessary; in the end, atpdec's (Leconte, 2003) values ensured good demodulation and image decoding results. The second demodulator is a simple envelope detector: the input signal gets full-wave rectified by the absolute value function and filtered by a linear-phase FIR filter with a steep transition between passband and stopband. The filter greatly attenuates the fc component while leaving the modulating signal intact. Demodulation quality is satisfactory at high SNR, though PLL demodulation shows better performance with low SNR signals. Furthermore, PLL demodulation has high computational complexity. On the other side, the software envelope detector solution has lower computational complexity; its hardware implementation is not easily accessible because it would require the addition of a low-pass filter with a large number of poles.

3.3.7 Synchronization Block

APT format is equipped with two synchronization pulses: horizontal synchronization (sync A) is used as a boundary between video lines and inter-channel synchronization (sync B) is used as a boundary between the two video channels (Winston, 1997). In our work, we only used sync A as we implemented channel separation in the Image Processing code by splitting every line into two parts, each consisting of 1040 pixels. Synchronization block processes signals sampled at a multiple of the symbol rate (4160 symbols/s), a requirement easily met by ADCs clocked by modern PLL clock generators. That being said, the signal is downsampled by selecting the median of the N samples instead of one sample every N. The median filter is widely known to greatly reduce impulse noise. Part (a) of Fig. 2 down-samples the signal, while (b) correlates previous part's output with a pattern of sync A; synchronization pulses are detected comparing local correlation peaks with maximum correlation in the last 3/4 seconds (c) (time during which one and a half video lines get transmitted). If correlation at discrete instant k-1 is a local peak and is greater than 80% of maximum correlation in said interval, it is considered as a synchronization pulse and a row formed by the last 2080 samples is inserted as a new element at the end of queue (e). Sometimes, synchronization pulses are lost or are erroneously detected due to signal fading or noise, so a filtering technique was devised (d): it filters pulses detected less than 2070 samples after last one. If a pulse has not been detected after 2090 samples the line is inserted at the end of the queue anyway and the 2090 samples counter is reset; the 2070 samples counter is not reset not to interfere with

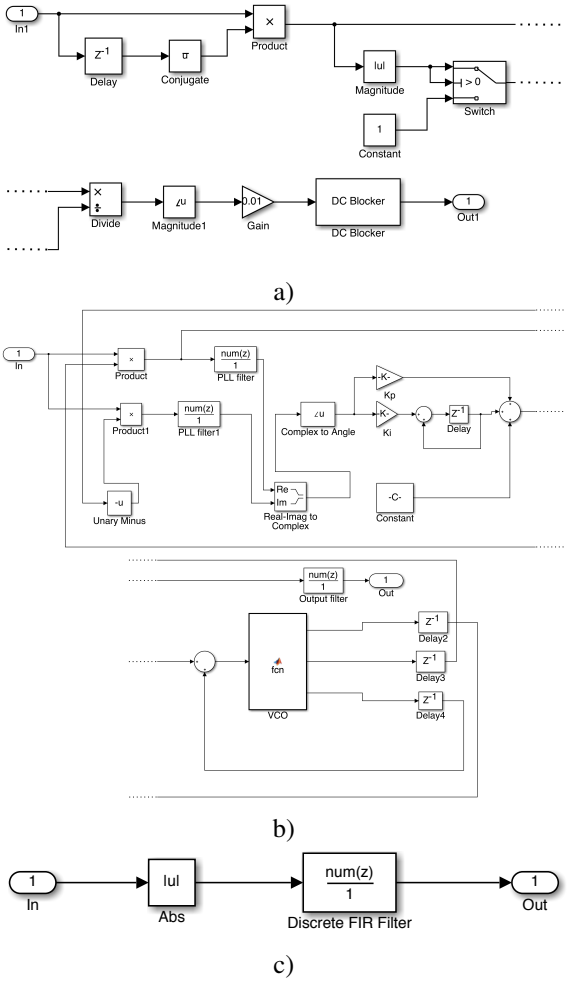

Figure 1: a) FM demodulator; b) PLL-based AM demodulator c) Envelope detector AM demodulator.

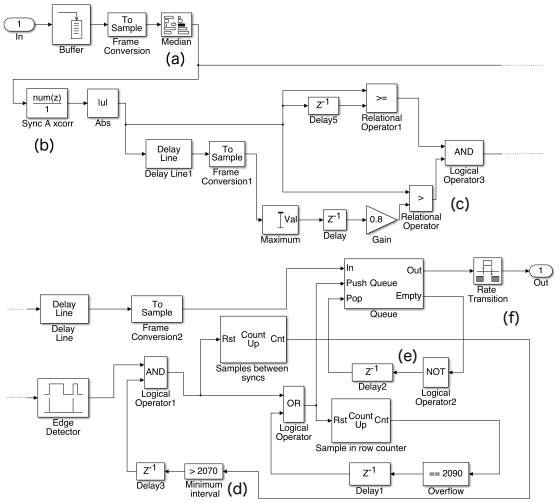

Figure 2: Synchronization block.

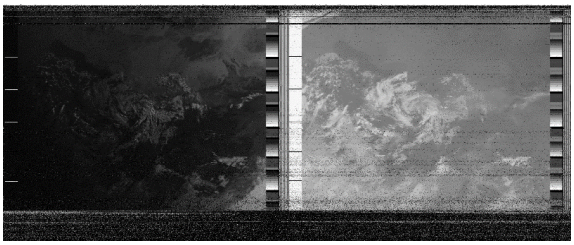

Figure 3: AVHRR image after automatic cropping.

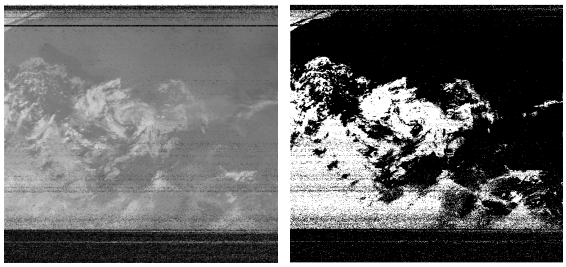

Figure 4: Left: disk filtered remote sensing image from NOAA. Right: clouds segmentation achieved with the Otsu method.

subsequent synchronization pulses. Finally, the Rate Transition block (f) outputs two lines of 2080 pixels each per second.

3.3.8 Pixel Dynamic Range Calibration Block

Each frame, composed of 128 rows, contains 16 wedges (or patches), the first nine carry data about the image dynamic range: wedges 1-8 represent values from 1/8 to 8/8, while 9 is the zero reference. The calibration block detects the exact position of those 9 wedges cross-correlating a vertical band of the image with an example pattern, then the values of wedges 8 and 9 are sampled to compute gray level offset and dynamic range. Offset is subtracted from pixel values and the result is divided by the detected dynamic range, in order, to normalize pixel values to the [0 1] interval: values outside this range can be treated as noise and clipped to 0 or 1. This block outputs a stream of pixel rows that can be further improved using Image Processing algorithms.

4 EXPERIMENTAL RESULTS

The output of our model is a 2080x2*T image, where T is running time in seconds. The image includes white noise or artifacts when PLL lock is not asserted, but these are cropped out by an algorithm using pixel variance in calibration wedges to estimate row reception quality. Only rows having an entropy below a certain threshold remain, of which an example is shown below (as a 2D plot). The result is a smaller image which uses less storage space and can be post-processed faster. As can be easily seen in Fig. 3, the image is corrupted by noise due to attenuation/fading of the satellite signal and intermodulation with strong out-of-band emissions, mainly from FM broadcasting transmitters and GSM base stations. Various Image Processing filtering methods have been used to enhance the images and objective metrics (PSNR and RMSE) allow us to compare the results. The results are reported in Table 1. The disk filter is shown to be achieving the best results of PSNR and RMSE. Once the image is denoised (Fig. 4 left), we used a state of the art cloud segmentation method to isolate clouds pixels both from land pixels and the rest of the image. Otsu method (Zhang and Hu, 2008) is a segmentation method widely used for its simpleness and effectiveness and its robustness against noise (usually present in APT images). That being said, our main objective was the release of a new accessible platform to receive NOAA signals and to enhance noisy images and achieve better results in terms of remote sensing imagery. We also show the results of clouds segmentation achieved by Otsu method (Fig. 4 right).

Table 1: Objective metrics results for image enhancement filtering.

Method	PSNR [dB]	RMSE
None (raw image)	17.788	0.129
3x3 arithmetic mean filter	17.981	0.126
3x3 geometric mean filter	13.655	0.208
3x3 harmonic mean filter	13.295	0.216
3x3 contraharmonic mean filter with Q = 1	18.023	0.126
3x3 gaussian filter	18.485	0.119
3x3 disk filter	18.590	0.118
Adaptive median filter (min: 3x3 - max: 5x5)	18.444	0.120
Adaptive filter 3x3	16.298	0.153

5 CONCLUSIONS AND FUTURE WORKS

In this paper we proposed a new easily accessible solution for NOAA remote sensing. Although we used low cost elements and hardware, we achieved good results in terms of signal reception, demodulation, synchronization and image enhancement. The system is able to predict NOAA satellite passes, lock, demodulate and synchronize the signals. The output of the demodulator is an image of the area scanned by a

line perpendicular to the flight direction of the NOAA satellite. We detected the clouds in the image by using Otsu method (Zhang and Hu, 2008). In future works we want to include the following solutions:

A more performant model for the receiver, such as FUNcube Dongle Pro+ or HackRF One; the adoption of a numerically controlled and built QFH antenna and an amplifier with lower noise figure and low signal loss; the development of an algorithm for thermal maps generation based on the analysis of the infrared images; noise profiling based on long time analysis of radio frequency interferences located near the receiver. We aim to develop a modular solution for the prediction of atmospheric phenomena, based on the analysis of the images retrieved from several satellites (each one transmitting at its own frequency and with its own modulation scheme) at different times of the day.

REFERENCES

Al-Moustafa, T., Armitage, R. P., and Danson, F. M. (2012). Mapping fuel moisture content in upland vegetation using airborne hyperspectral imagery. *Remote sensing of Environment*, 127:74–83.

Alkhatib, M. Q., Cabrera, S. D., and Gill, T. E. (2012). Automated detection of dust clouds and sources in NOAA-AVHRR satellite imagery. In *Image Analysis and Interpretation (SSIAI), 2012 IEEE Southwest Symposium on*, pages 97–100. IEEE.

Barnes, J. C. and Smallwood, M. D. (1982). Tiros-N series direct readout services users guide.

Benabadji, N., Hassini, A., and Belbachir, A. H. (2004). Hardware and software consideration to use NOAA images. *Revue Internationale des Energies Renouvelables, CDER*, 7(01):1–11.

Camps-Valls, G., Benediktsson, J. A., Bruzzone, L., and Chanussot, J. (2011). Introduction to the issue on advances in remote sensing image processing. *IEEE Journal of Selected Topics in Signal Processing*, 5(3):365–369.

Farserotu, J. and Prasad, R. (2000). A survey of future broadband multimedia satellite systems, issues and trends. *IEEE Communications Magazine*, 38(6):128–133.

Feidas, H., Cartalis, C., and Cracknell, A. (2000). Use of Meteosat imagery to define clouds linked with floods in Greece. *International Journal of Remote Sensing*, 21(5):1047–1072.

Griffiths, M. (2014). Turnstile design — DigitalHam. http://www.digitalham.co.uk/design.

Heidinger, A. K., Evan, A. T., Foster, M. J., and Walther, A. (2012). A naive Bayesian cloud-detection scheme derived from CALIPSO and applied within PATMOS-x. *Journal of Applied Meteorology and Climatology*, 51(6):1129–1144.

Karlsson, K.-G., Johansson, E., and Devasthale, A. (2015). Advancing the uncertainty characterisation of cloud masking in passive satellite imagery: Probabilistic formulations for NOAA AVHRR data. *Remote Sensing of Environment*, 158:126–139.

Keen, K. (2013). Rtl_fm Guide: Updates for rtl_fm overhaul. http://kmkeen.com/rtl-demod-guide.

Leconte, T. (2003). ATPDEC Home Page. http://atpdec.sourceforge.net.

Lyons, R. G. (2004). *Understanding Digital Signal Processing, 3/E*. Pearson Education India.

Magliacane, J. (2001). PREDICT - A Satellite Tracking/Orbital Prediction Program. http://www.qsl.net/kd2bd/predict.html.

Moradi, I., Meng, H., Ferraro, R. R., and Bilanow, S. (2013). Correcting geolocation errors for microwave instruments aboard NOAA satellites. *IEEE Transactions on Geoscience and Remote Sensing*, 51(6):3625–3637.

Osmocom (2012). rtl-sdr - OsmoSDR. http://sdr.osmocom.org/trac/wiki/rtl-sdr.

Promwong, S. and Takada, J.-i. (2004). Free space link budget estimation scheme for ultra wideband impulse radio with imperfect antennas. *IEICE Electronics Express*, 1(7):188–192.

Sergienko, A. B. (2014). Software-defined radio in MATLAB Simulink with RTL-SDR hardware. In *Computer Technologies in Physical and Engineering Applications (ICCTPEA), 2014 International Conference on*, pages 160–161. IEEE.

Shima, J. M. (1995). FM demodulation using a digital radio and digital signal processing. Master's thesis, University of Florida.

Simpson, J. J. and Gobat, J. I. (1996). Improved cloud detection for daytime AVHRR scenes over land. *Remote Sensing of Environment*, 55(1):21–49.

Sruthi, M., Abirami, M., Manikkoth, A., Gandhiraj, R., and Soman, K. (2013). Low cost digital transceiver design for Software Defined Radio using RTL-SDR. In *Automation, Computing, Communication, Control and Compressed Sensing (iMac4s), 2013 International Multi-Conference on*, pages 852–855. IEEE.

Wilson, J., Nelson, A., and Farhang-Boroujeny, B. (2009). Parameter derivation of type-2 discrete-time phase-locked loops containing feedback delays. *IEEE Transactions on Circuits and Systems II: Express Briefs*, 56(12):886–890.

Winston, W. (1997). User's Guide for Building and Operating Environmental Satellite Receiving Stations. *National Environmental Satellite, Data, and Information Service, NOAA*.

Yhann, S. R. and Simpson, J. J. (1995). Application of neural networks to AVHRR cloud segmentation. *IEEE transactions on geoscience and remote sensing*, 33(3):590–604.

Zhang, J. and Hu, J. (2008). Image segmentation based on 2D Otsu method with histogram analysis. In *Computer Science and Software Engineering, 2008 International Conference on*, volume 6, pages 105–108. IEEE.